Organic &
Biomolecular
Chemistry

Halide selective anion recognition by an amide-triazolium axle containing [2]rotaxane

Halide selective anion recognition by an amide-triazolium axle containing [2]rotaxane

Nicholas G. White,[a] Ana R. Colaço,[b] Igor Marques,[b] Vítor Félix[b] and Paul D. Beer[a*]

A new rotaxane containing the 3-amido-phenyl-triazolium group incorporated into the interlocked structure's axle component has been prepared by a chloride anion templated clipping strategy. Proton NMR titration experiments reveal that the interlocked host displays a high degree of halide anion recognition in competitive 1:1 $CDCl_3:CD_3OD$ solvent mixture. Chloride and bromide anions are bound strongly and selectively, with negligible complexation of the larger, more basic oxoanions, acetate and dihydrogen phosphate being observed. Density functional theory calculations on related axle motifs 3-amido-phenyl-triazolium, pyridinium bis-triazole and pyridinium bis-amide were performed, and indicated that the new rotaxane axle motif displays much weaker oxoanion binding than the pyridinium based systems.

Introduction

Inspired by the key roles played by anions in numerous biological and environmental processes,[1] the development of artificial anion receptors is an area of intense current research interest.[2] Seminal reports in 2008 established that readily-prepared 1,2,3-triazole groups could bind anions through polarized C–H hydrogen bonds,[3] and a range of triazole containing hosts have since been reported,[4] as well as a few receptors containing the alkylated *triazolium* moiety.[5]

Notably, Pandey has utilized a bile acid scaffold to synthesize a range of acyclic and macrocyclic bis-triazolium systems that selectively bind fluoride, chloride, hydrogen sulfate or dihydrogen phosphate, depending on the host structure.[5a,d,e] Inspired by this work, we prepared a triazolium axle containing rotaxane[6] *via* anion templation, and demonstrated that this interlocked host could bind anions in competitive solvent media.[5b] More recently, we have reported a tetra-triazolium macrocycle[5f] and tetra-triazolium cage,[5g] and demonstrated that these highly charged receptors exhibit strong recognition of sulfate in aqueous mixtures.
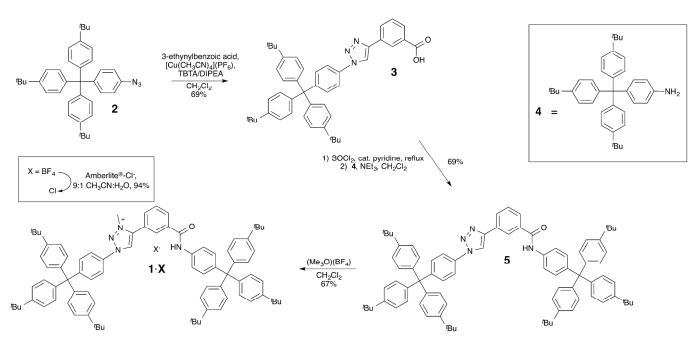
Herein we introduce the novel 3-amido-phenyl-triazolium motif, containing both amide and triazolium functionality.[7] By incorporating this motif into an axle component, we demonstrate its use in the anion templated synthesis of a novel rotaxane host system which exhibits a notably high degree of halide anion recognition over oxoanions in competitive 1:1 $CDCl_3:CD_3OD$ solvent mixtures. This anion selectivity trend is rationalised by computational experiments on anion complexes of the rotaxane's amido-phenyl-triazolium axle component which indicate this motif to be a relatively weak binder of oxoanions when compared with bis-triazole and bis-amide pyridinium containing axles.

Results and discussion

Rotaxane synthesis

The triazolium-amide containing axle component **1**[+] was prepared in three steps from commercially available 3-ethynylbenzoic acid (Scheme 1). Copper(I)-catalyzed azide-alkyne cycloaddition (CuAAC) reaction of azide-appended tetraphenyl compound **2**[8] gave acid **3** in 69% yield. Activation of the acid using refluxing thionyl chloride, followed by condensation with tetraphenyl amine **4**[9] afforded the triazole-amide axle component **5**, again in 69% yield. Alkylation using trimethyloxonium tetrafluoroborate in dry dichloromethane, followed by anion exchange using Amberlite® resin produced the triazolium-amide axle component **1**·Cl.
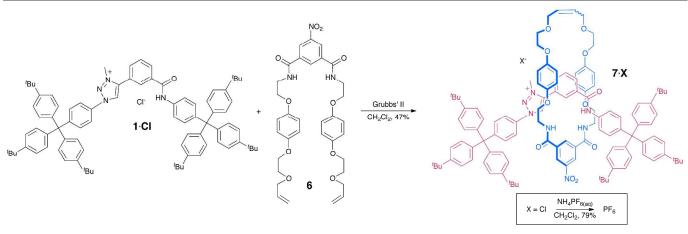
Scheme 1 Synthesis of triazolium-amide containing axle component **1·Cl**.

Grubbs'-catalysed chloride anion templated ring closing metathesis of **1·Cl** and bis-vinyl macrocycle precursor **6**[10] in dichloromethane followed by purification *via* preparative TLC and recrystallization gave rotaxane **7·Cl** in 47% yield (Scheme 2). Anion exchange to **7·PF₆** was achieved by repeated washing with aqueous NH₄PF₆(aq).
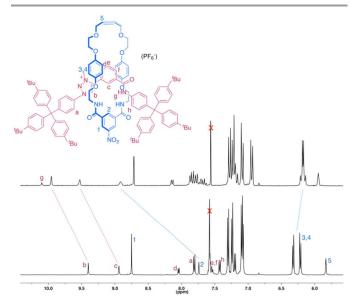
The new rotaxane was characterized by ¹H, ¹³C, ¹⁹F and ³¹P NMR spectroscopy, as well as by high resolution ESI mass spectrometry. The interlocked nature of the compound was also confirmed by 2D ROESY spectroscopy (Figure S13). The ¹H NMR spectra of the chloride and hexafluorophosphate salts

of **7⁺** are shown in Figure 1: the host's cavity resonances b, c and 2 are observed significantly downfield in **7·Cl** compared to **7·PF₆**, consistent with hydrogen bonding interactions between these protons and the interlocked cavity encapsulated halide anion. The hydroquinone signals, 3 and 4, are shifted upfield relative to the hexafluorophosphate salt, suggesting enhanced pyridinium···hydroquinone aromatic donor–acceptor interactions upon anion coordination.

Scheme 2 Synthesis of triazolium-amide axle containing rotaxane **7·PF₆**.

Fig. 1 Partial ^{1}H NMR spectra of **7·PF₆** (bottom) and **7·Cl** (top). Peak labelled × corresponds to residual CHCl₃ signal, unlabelled peaks belong to bulky stopper groups (1:1 CDCl₃:CD₃OD, 293 K).

Small single crystals of the rotaxane as its bromide salt were obtained from a ^{1}H NMR titration sample (*vide infra*) suitable for synchrotron X-ray structural analysis. The bromide anion is held within the interlocked cavity (Figure 2) by hydrogen bonds from triazolium, amide and macrocycle phenylene protons. In the solid state, hydrogen bonds from the axle triazolium and amide groups are of moderate strength, while the anion sits asymmetrically within the macrocycle, forming one strong and one weak hydrogen bond to amide donors from the cycle (more details are given in the Supporting Information). Donor–acceptor interactions are observed between one of the macrocycle's hydroquinone rings and the central phenylene ring of the axle component [centroid⋯centroid = 3.660(17) Å], with a longer contact between the other hydroquinone ring and the triazolium group [centroid⋯centroid = 3.813(9) Å].
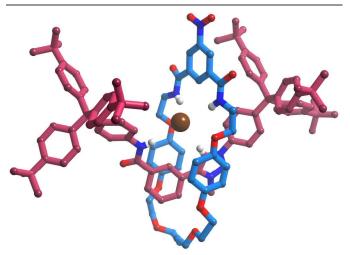

Fig. 2 X-ray crystal structure of **7·Br**. Minor component of the disordered macrocycle and most hydrogen atoms are omitted for clarity.
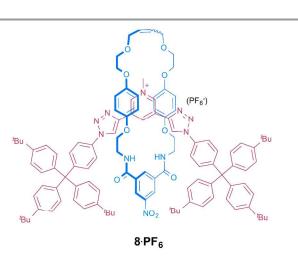
Rotaxane anion binding

The anion recognition properties of **7·PF₆** were investigated using ^{1}H NMR titration experiments in competitive 1:1 CDCl₃:CD₃OD solvent mixture (see ESI for titration protocols and data). WINEQNMR2[11] analysis of the titration data determined 1:1 stoichiometric association constants, monitoring the rotaxane's triazolium resonance (Table 1).
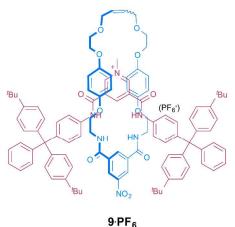
Table 1 Association constants, K_a (M^{-1}), for rotaxanes with halide and polyatomic anions in 1:1 CDCl₃:CD₃OD.

Anion	**7·PF₆**[a]	**8·PF₆**[8]	**9·PF₆**[10,c]
Cl⁻	2035(50)	411(18)	4500
Br⁻	1948(15)	936(40)	—[d]
H₂PO₄⁻	—[b]	186(9)	1500
OAc⁻	—[b]	137(3)	725

[a]Anions added as tetrabutylammonium salts, estimated standard errors given in parentheses, association constants determined using WINEQNMR[11] at 293 K. [b]Peak shifts too small to infer binding event (< 0.05 ppm after 10 equivalents of anion). [c]Errors estimated to be less than 10%. [d]No data reported.

Both chloride and bromide anions are bound strongly by the rotaxane, with addition of chloride causing significantly larger shifts than bromide. When the oxoanions acetate and dihydrogen phosphate are added to the receptor, only very small movements of the ^{1}H NMR signals were observed (less than 0.05 ppm over the course of the titration experiments), suggesting negligible anion binding. The selectivity for the halide anions over the more basic oxoanions is noteworthy, and presumably arises due to the preorganised three-dimensional cavity of the interlocked host, which is too small to accommodate the large oxoanions.

The pronounced chloride and bromide selectivity of **7·PF₆** is particularly noteworthy when compared with the analogous rotaxanes **8·PF₆**[8] and **9·PF₆**[10] (Figure 3), which contain an identical macrocycle to **7·PF₆** and respectively pyridinium bis-triazole and pyridinium bis-amide axle components. While both **8·PF₆** and **9·PF₆** display selectivity for halide anions over oxoanions, significant oxoanion binding *is* still observed, which is not the case with **7·PF₆** (Table 1). Further insight into these results was obtained by quantum calculations, as described below.
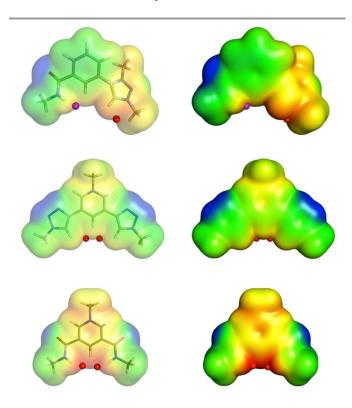
8·PF$_6$

9·PF$_6$

Fig. 3 Structures of rotaxanes related to **7·PF$_6$**, **8·PF$_6$**[8] and **9·PF$_6$**.[10]

Fig. 4 Computed electrostatic potentials mapped on the 0.001 electrons/Bohr^3 surface of **7$_{methyl}$**$^+$ (top), **8$_{methyl}$**$^+$ (middle) or **9$_{methyl}$**$^+$ (bottom), with colours ranging between blue (< 31.4 kcal mol^{-1}) and red (> 125.5 kcal mol^{-1}). The locations of $V_{S,max}$ are illustrated with red and purple dots.

of the electrostatic potential on the surfaces of these molecules. However, the $V_{S,max}$ values computed for the hypothetical molecules mirror the trend observed for the complete axles, indicating that this quantum descriptor is mainly dictated by the central core of the axle component.

DFT calculations on truncated axle motifs

The electrostatic potential computed on a molecule's electron density surface (V_S) is an excellent tool to evaluate non-covalent interactions that have a significant electrostatic contribution.[12] In particular, the most positive values ($V_{S,max}$) are straightforwardly related to hydrogen-bond acidity[13] and consequently with the receptor's anion binding ability.[14] In this context, the structures of the axle components of the interlocked hosts **7**$^+$, **8**$^+$ and **9**$^+$ were optimised at B3LYP/6-31G** followed by calculation of the $V_{S,max}$ at the same level of theory with Gaussian 09.[15] In addition, the $V_{S,max}$ were computed for the 3-amido-phenyl-triazolium, pyridinium bis-triazole and pyridinium bis-amide axle motifs generated from the corresponding axles by the complete replacement of the tetraphenyl stoppers by methyl substituents. DFT calculations on these hypothetical molecules, denoted as **7$_{methyl}$**$^+$, **8$_{methyl}$**$^+$ and **9$_{methyl}$**$^+$, allow us to ascertain the axle motifs' contribution to the electrostatic potential of the entire axle component.

The $V_{S,max}$ for the axles of **7**$^+$, **8**$^+$ and **9**$^+$ are gathered in Table 2 together with those calculated for the corresponding motifs **7$_{methyl}$**$^+$, **8$_{methyl}$**$^+$ and **9$_{methyl}$**$^+$. Overall, the $V_{S,max}$ values for the complete axles are lower than the corresponding central motif values, as would be expected for the different distribution

The electrostatic potential mapped on the electronic density surfaces of each central motif is shown in Figure 4, along with the position of $V_{S,max}$. Equivalent depictions are presented in Figure S16 for the entire axle components. The symmetric **8$_{methyl}$**$^+$ and **9$_{methyl}$**$^+$ entities exhibit two distinct $V_{S,max}$ (single red dots) with almost identical energies located in the region of the two binding sites (C$_{triazole}$–H or N–H amide groups). In contrast, the **7$_{methyl}$**$^+$ axle motif, with an asymmetric structure, presents a higher $V_{S,max}$ of 116.57 kcal mol^{-1} near the C–H from the positively charged triazolium ring (red dot) and a second one, with a lower energy of 106.81 kcal mol^{-1} (purple dot) close to the N–H binding site. In other words, this entity, like the complete axle component **7**$^+$, exhibits two binding sites with different acidities and, therefore, with different anion affinities.

The binding ability of the neutral macrocycle was also computed at the same theory level (see ESI for details), affording two close $V_{S,max}$ of 45.93 and 43.10 kcal mol^{-1}, which are situated in the vicinity of the N–H binding units of the isophthalamide head (red dots in Figure S17). Given that the same macrocycle is present in rotaxanes **7**$^+$, **8**$^+$ and **9**$^+$, it would seem reasonable that differences in binding strength are largely

due to variation in the axle component,[16] and so we focussed our modelling on this part of the interlocked structure.

The $V_{S,max}$ listed in Table 2 are in perfect agreement with the experimental binding data, following the anion affinity order $9^+ > 7^+ > 8^+$, as given by the association constants for chloride anion. To investigate the observed selectivity preference of 7^+, we next modelled the hydrogen bonding arrangements between the three axle motifs and the four anions under study (Cl⁻, Br⁻, $H_2PO_4^-$ and OAc⁻).

Table 2 $V_{S,max}$ (kcal mol⁻¹) calculated for complete and truncated axle components at B3LYP/6-31G**.

Structure	Entire axle[a]	Truncated motif[b]
7^+	108.76,[c] 102.74	116.57,[c] 106.81
8^+	99.51, 97.80	106.82, 106.52
9^+	122.43, 120.26	129.31, 129.02

[a]Starting geometries of the axle components were taken from the single crystal X-ray structures of related rotaxane systems, as described in the ESI. [b]Truncated motif corresponds to the axle fragments 7_{methyl}^+, 8_{methyl}^+ or 9_{methyl}^+ as defined in the text. [c]This $V_{S,max}$ corresponds to the $C_{triazolium}$–H site.

The complexes between axle motifs 7_{methyl}^+, 8_{methyl}^+ and 9_{methyl}^+, and the four inorganic anions were optimised using the B3LYP functional and the basis set 6-311+G**. The use of these structural motifs rather than the entire axles components is computationally less demanding and is appropriate given that the axles' electrostatic potential is largely determined by the central motif (*vide supra*). The final geometries of the anion complexes with 7_{methyl}^+ are shown in Figure 5 together with the intermolecular hydrogen bonds. Similar depictions are presented in Figures S18 and S19 for the anion complexes with 8_{methyl}^+ and 9_{methyl}^+. The distances of two relevant hydrogen bonds between the binding units and the anions are given in Table 3 along with the second order stabilization energies (E^2)[17] between the anions' lone pairs and anti-bonding orbitals of the axle motif (σ* N–H or C–H orbitals). The complete dimensions of all intermolecular bonding interactions for all three axle motifs are summarised in Tables S1–S3.

When considering the halide anions, the shortest hydrogen bonds are observed between 9_{methyl}^+ and the anions, while 8_{methyl}^+ forms the longest hydrogen bonds, and 7_{methyl}^+ is intermediate between 9_{methyl}^+ and 8_{methyl}^+. These hydrogen bond dimensions lead to E^2 stabilization energies for the halide anions following the trend $9_{methyl}^+ > 7_{methyl}^+ > 8_{methyl}^+$. These trends are entirely in accordance with the solution phase anion binding data for the related rotaxane host systems and the calculated $V_{S,max}$ values.

Interestingly though, 7_{methyl}^+ forms much longer hydrogen bonds to the oxoanions than 9_{methyl}^+ and comparable (OAc⁻) or longer ($H_2PO_4^-$) hydrogen bonds than 8_{methyl}^+. The E^2 values for these anions are highest for 9_{methyl}^+, slightly lower for 8_{methyl}^+ and much lower for 7_{methyl}^+. Taken together these results demonstrate that the central motif of 7^+ has a much weaker affinity for oxoanions than those present in 8^+ or 9^+, and corroborate the negligible solution binding of oxoanions by rotaxane 7^+.

While in general, the oxoanions $H_2PO_4^-$ and OAc⁻ form shorter hydrogen bonds with the axle motifs than the halide anions, suggesting stronger binding, this analysis neglects the key contributing factor of the preorganised three-dimensional interlocked cavity. It has been previously observed experimentally[18] that the axle component of 9^+ displays a strong preference for basic oxoanions over chloride, but the formation of the rotaxane host structure overcomes, and indeed reverses, this trend. Given the computed weaker oxoanion binding of the axle motif of 7^+, it seems that rotaxane formation leads to almost complete loss of binding for these large oxoanions in the competitive solvent media used. This feature is being investigated further by means of classical molecular dynamics simulations on twelve host–guest complexes formed between rotaxanes 7^+, 8^+ and 9^+ and the anions Cl⁻, Br⁻, OAc⁻ and $H_2PO_4^-$, and the results of this computational study will be reported in due course.
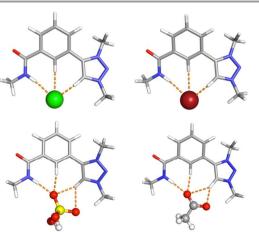

Fig. 5 DFT optimized geometries at B3LYP/6-311+G** of the monoatomic (top) and polyatomic (bottom) anion complexes with the 7_{methyl}^+ axle motif.

Table 3 Hydrogen bond distances (Å) of two relevant interactions between the truncated axle motifs and anions (X⁻), along with the corresponding second order stabilization energies (E^2, kcal mol^{-1}).

| Anion | 7_{methyl}^+ | | | | 8_{methyl}^+ | | | 9_{methyl}^+ | |
	$C\cdots X^-$	$N\cdots X^-$	E^2	$C\cdots X^-$	$C\cdots X^-$	E^2	$N\cdots X^-$	$N\cdots X^-$	E^2
Cl⁻	3.377	3.191	40.38	3.417	3.418	29.45	3.219	3.220	45.38
Br⁻	3.575	3.328	32.16	3.573	3.573	27.02	3.381	3.382	35.50
$H_2PO_4^-$	3.175	2.896	24.62	2.936	2.976	60.18	2.691	2.711	66.75
OAc⁻	2.914	2.879	30.20	2.924	2.948	47.78	2.686	2.709	69.41

Conclusions

In summary, a new rotaxane incorporating the 3-amido-phenyl-triazolium motif has been prepared by an anion templation methodology. The interlocked host is selective for halide anions over the larger, more basic oxoanions, acetate and dihydrogen phosphate. Importantly, this selectivity is far more pronounced than that reported for analogous rotaxanes incorporating pyridinium bis-triazole or pyridinium bis-amide axle components. Molecular modelling studies suggest that this is due to the amido-phenyl-triazolium motif exhibiting inherently weaker oxoanion binding than the pyridinium containing motifs.

Experimental

General remarks

General comments, details of instrumentation, ^{1}H NMR and ^{13}C NMR spectra of new compounds are provided in the Supporting Information.

X-ray crystallography

Diffraction data were collected at Diamond Lightsource, Beamline I19[19] (λ = 0.6889 Å), at 100 K.[20] Raw frame data, including data reduction, inter-frame scaling, unit cell refinement and absorption corrections were processed using CrysAlisPro.[21] The structure was solved with SIR92[22] and refined using full-matrix least-squares on F^2 within the CRYSTALS suite.[23] All non-hydrogen atoms were refined with anisotropic displacement parameters; hydrogen atoms were generally visible in the difference map, and were refined with restraints on bond lengths and angles, after which the positions were used as the basis for a riding model.[24] Crystals were found to be twinned – an appropriate twin law was found using the ROTAX[25] package within the CRYSTALS suite. Full crystallographic details are provided in CIF format as Supporting Information.

Triazole acid 3

The aryl azide 2^8 (0.106 g, 0.200 mmol) and 3-ethynylbenzoic acid (0.037 g, 0.25 mmol) were dissolved in CH_2Cl_2 (10 mL). DIPEA (0.090 mL, 0.065 g, 0.50 mmol), TBTA (0.011 g, 0.020 mmol) and [Cu(CH$_3$CN)$_4$](PF$_6$) (0.0075 g, 0.020 mmol) were added and the yellow solution stirred at room temperature under a nitrogen atmosphere for 3 days. The reaction was

diluted with further CH_2Cl_2 (10 mL), washed with HCl$_{(aq)}$ (1 M, 2 × 20 mL) and brine (20 mL), dried (MgSO$_4$), and taken to dryness under reduced pressure. Column chromatography (5% CH$_3$OH in CH_2Cl_2) gave **3** as a white powder. Yield: 0.093 g (69%).

^{1}H NMR (d$_6$-DMSO): 9.36 (s, 1H, trz-*H*), 8.51 (s, 1H, ph-*H*), 8.16 (d, ^3J = 7.8 Hz, 1H, ph-*H*), 7.94 (d, ^3J = 7.8 Hz, 1H, ph-*H*), 7.88 (d, ^3J = 8.7 Hz, 2H, stopper-*H*), 7.62 (app. t, ^3J = 7.8 Hz, 1H, ph-*H*), 7.33–7.41 (m, 8H, stopper-*H*), 7.15 (d, ^3J = 8.5 Hz, 6H, stopper-*H*), 1.26 (s, 27H, ^{t}Bu-*H*). ^{13}C (d$_6$-DMSO): 148.1, 147.7, 146.5, 143.4, 134.2, 131.7, 130.6 130.0, 129.4, 129.4, 129.0, 129.0, 126.0, 124.7, 120.1, 119.5, 63.2, 34.1, 31.1 (one resonance overlapping/not observed). HRESI-MS (neg.): 674.3757, calc. for [C$_{46}$H$_{48}$N$_3$O$_2$]$^-$ = 674.3752.

Triazole axle 5

The carboxylic acid **3** (0.068 g, 0.10 mmol) was suspended in SOCl$_2$ (2 mL). A drop of pyridine was added, and the suspension was heated to reflux under a nitrogen atmosphere for 16 hours, during which time all material dissolved. The SOCl$_2$ was removed under reduced pressure and the resulting yellow solid taken up in dry CH_2Cl_2 (10 mL). NEt$_3$ (0.056 mL, 0.040 g, 0.40 mmol) was added followed by the tetraphenyl amine 4^9 in dry CH_2Cl_2 (10 mL), and the resulting clear yellow solution was stirred at room temperature under a nitrogen atmosphere for 16 hours. It was washed with 10% HCl$_{(aq)}$ (2 × 20 mL) and brine (20 mL), dried (MgSO$_4$), and taken to dryness under reduced pressure. Column chromatography (CH_2Cl_2) gave **5** as a white powder. Yield: 0.080 g (69%).

^{1}H NMR (CDCl$_3$): 8.39 (s, 1H, amide-*H*), 8.25 (s, 1H, trz-*H*), 8.07 (d, ^3J = 8.0 Hz, 1H, phenyl-*H*), 8.01 (s, 1H, phenyl-*H*), 7.86 (d, ^3J = 7.7 Hz, 1H, phenyl-*H*), 7.65 (d, ^3J = 8.8 Hz, 2H, stopper-*H*), 7.54–7.59 (m, 3H, 1 × phenyl-*H*, 2 × stopper-*H*), 7.42 (d, ^3J = 8.8 Hz, 2H, stopper-*H*), 7.21–7.29 (m, 14H, stopper-*H*), 7.10–7.14 (m, 12H, stopper-*H*), 1.32 (s, 27H, ^{t}Bu-*H*), 1.31 (s, 27H, ^{t}Bu-*H*). ^{13}C NMR (CDCl$_3$): 165.4, 148.9, 148.5, 144.0, 143.4, 135.9, 135.6, 134.5, 132.7, 132.0, 131.0, 130.8, 130.8, 130.6, 129.6, 129.1, 127.2, 124.8, 124.8, 124.5, 124.3, 119.5, 119.1, 118.3, 118.3, 63.7, 63.5, 34.5, 34.5, 31.5 (one resonance overlapping/not observed). HRESI MS (pos.): 1183.7157, calc. for [C$_{83}$H$_{92}$NO$_4$·Na]$^+$ = 1183.7163.

Triazolium axle component 1^+

The triazole axle component **5** (0.058 g, 0.050 mmol) was dissolved in dry CH_2Cl_2 (10 mL). (Me$_3$O)(BF$_4$) (0.0088 g, 0.060 mmol) was added and the mixture stirred at room

temperature under a nitrogen atmosphere for 16 hours. The alkylating agent was quenched by addition of CH_3OH (1 mL), and the colourless solution taken to dryness under reduced pressure. Column chromatography (5% CH_3OH in CH_2Cl_2) gave **1·BF$_4$** as a white powder. Yield: 0.042 g (67%).

^{1}H NMR ($CDCl_3$): 9.15 (s, 1H, amide-H), 9.07 (s, 1H, trz$^+$-H), 8.21 (s, 1H, phenyl-H), 8.01 (d, ^3J = 7.9 Hz, 1H, phenyl-H), 7.61–7.73 (m, 5H, 4 × stopper-H, 1 × phenyl-H), 7.49 (d, ^3J = 8.9 Hz, 2H, stopper-H), 7.40 (app. t, ^3J = 7.9 Hz, 1H, phenyl-H), 7.09–7.30 (m, 26H, stopper-H), 4.27 (s, 3H, methyl-H), 1.31 (s, 27H, ^{t}Bu-H), 1.29 (s, 27H, ^{t}Bu-H). ^{13}C NMR (d$_6$-DMSO): 164.4, 151.0, 148.3, 147.8, 143.8, 143.0, 142.6, 142.4, 136.4, 136.1, 132.3, 132.2, 132.1, 130.6, 130.4, 130.0, 129.9, 129.7, 129.1, 127.7, 124.8, 124.5, 122.9, 120.9, 119.7, 63.4, 62.9, 34.1, 34.1, 31.3, 31.3 (one peak obscured by DMSO signal). ^{19}F NMR (d$_6$-DMSO): −148.3 (m). HRESI-MS (pos.): 1175.7475, calc. for $[C_{84}H_{95}N_4O]^+$ = 1175.7500.

The tetrafluoroborate salt of **1$^+$** (0.032 g, 0.025 mmol) was taken up in 9:1 CH_3CN:H_2O (50 mL, required gentle heating). It was repeatedly passed down a Cl$^−$-loaded Amberlite$^®$ anion exchange column. The CH_3CN was removed under reduced pressure and the remaining aqueous suspension extracted with CH_2Cl_2 (3 × 20 mL). The combined organic fractions were washed with brine (20 mL), dried (MgSO$_4$), and taken to dryness under reduced pressure to give **1·Cl** as a sparingly-soluble white powder. Yield: 0.029 g (94%).

^{1}H NMR (5:1 $CDCl_3$:CD_3OD): 9.79 (s, 1H, trz$^+$-H), 8.49 (s, 1H, phenyl-H), 8.20 (d, ^3J = 7.8 Hz, 1H, phenyl-H), 7.82–7.89 (m, 3H, 2 × stopper-H, 1 × phenyl-H), 7.68–7.75 (m, 3H, 2 × stopper-H, 1 × phenyl-H), 7.53 (d, ^3J = 8.9 Hz, 2H, stopper-H), 7.15–7.27 (m, 14H, stopper-H), 7.04–7.10 (m, 12H, stopper-H), 4.44 (s, 3H, methyl-H), 1.27 (s, 27H, ^{t}Bu-H), 1.26 (s, 27H, ^{t}Bu-H). LRESI-MS (pos.): 1175.77, calc. for $[C_{84}H_{95}N_4O]^+$ = 1175.75.

Rotaxane 7$^+$

The chloride salt of **1$^+$** (0.024 g, 0.020 mmol) and the bis-vinyl precursor **6**^{10} (0.020 g, 0.030 mmol) were dissolved in dry CH_2Cl_2 (5 mL, required gentle heating). Grubbs' II catalyst (0.0020 g, 10% by weight) was added and the reaction stirred at room temperature under a nitrogen atmosphere for 3 days. It was taken to dryness under reduced pressure, and purified by preparative TLC (2% CH_3OH in CH_2Cl_2) to give slightly impure **7$^+$** (yield at this point ~ 0.021 g, ~ 57%). It was taken up in hot CH_3OH/CH_2Cl_2 (4:1, 10 mL), and the total volume reduced to ~ 5 mL by boiling. Cooling the solution resulted in the precipitation of a white powder, which was isolated by filtration and washed with ice-cold CH_3OH (2 × 1 mL) to give **7·Cl**. Yield: 0.017 g (47%).

^{1}H NMR (1:1 $CDCl_3$:CD_3OD): 10.10 (s, 1H, amide-H), 9.96 (s, 1H, trz$^+$-H), 9.53 (s, 1H, phenyl-H), 8.92 (s, 1H, phenyl-H), 8.72 (s, 2H, phenyl-H), 8.14 (d, ^3J = 7.4 Hz, 1H, phenyl-H), 7.63–7.87 (m, 8H, 4 × stopper-H, 2 × amide-H, 2 × phenyl-H), 7.16–7.30 (m, 20H, stopper-H) 7.09 (d, ^3J = 8.5 Hz, 6H, 6 stopper-H), 6.95 (d, ^3J = 8.5 Hz, 6H, stopper-H), 6.14–6.22 (m, 8H, hydroquinone-H), 5.95 (app. br. s, 2H, vinyl-H), 4.32 (s,

3H, methyl-H), 3.61–4.16 (m, 20H, macrocycle-CH_2), 1.33 (s, 27H, ^{t}Bu-H), 1.27 (s, ^{t}Bu-H). HRESI-MS (pos.): 1796.9870, calc. for $[C_{116}H_{130}N_7O_{11}]^+$ = 1796.9823.

The chloride salt of **7$^+$** (0.014 g, 0.0075 mmol) was taken up in CH_2Cl_2 (20 mL). The solution was washed with $NH_4PF_{6(aq)}$ (0.1 M, 7 × 20 mL) and H_2O (3 × 20 mL). Thorough drying in vacuo gave **7·PF$_6$** as a white powder. Yield: 0.012 g (79%).

^{1}H NMR (1:1 $CDCl_3$:CD_3OD): 9.40 (s, 1H, trz$^+$-H), 8.94 (s, 1H, phenyl-H), 8.75 (d, ^4J = 1.5 Hz, 2H, phenyl-H), 8.04 (d, ^3J = 7.9 Hz, 1H, phenyl-H), 7.81 (d, ^3J = 8.8 Hz, 2H, stopper-H), 7.74 (t, ^4J = 1.5 Hz, 1H, phenyl-H), ~ 7.59 (obscured by residual CHCl$_3$ peak, 1H, phenyl-H), 7.55 (app. t, ^3J = 7.9 Hz, 1H, phenyl-H), 7.43 (d, ^3J = 8.8 Hz, 2H, stopper-H), 7.30 (d, ^3J = 8.7 Hz, 6H, stopper-H), 7.24 (d, ^3J = 8.9 Hz, 6H, stopper-H), 7.20 (d, ^3J = 8.9 Hz, 2H, stopper-H), 7.07–7.10 (m, 14H, stopper-H), 6.21–6.33 (m, 8H, hydroquinone-H), 5.83 (app. br. s, 2H, vinyl-H), 4.19 (s, 3H, methyl-H), 3.43–4.00 (m, 20H, macrocycle-CH_2), 1.32 (s, 27H, ^{t}Bu-H), 1.29 (s, 27H, ^{t}Bu-H). ^{13}C NMR (1:1 $CDCl_3$:CD_3OD): 165.9, 165.7, 153.3, 153.1, 149.8, 149.2, 149.1, 145.1, 144.6, 143.5, 143.3, 136.6, 136.5, 136.1, 133.5, 132.7, 132.2, 131.7, 131.2, 131.0, 130.2, 130.1, 129.7, 127.0, 126.1, 125.3, 124.8, 122.4, 120.7, 120.2, 115.6, 115.0, 71.4, 69.8, 68.4, 66.9, 64.6, 64.1, 40.6, 40.1, 34.9, 34.8, 31.7, 31.6 (3 resonances overlapping/not observed). ^{19}F NMR (1:1 $CDCl_3$:CD_3OD): −73.4 (d, $^2J_{P,F}$ = 711 Hz). ^{31}P NMR (1:1 $CDCl_3$:CD_3OD): −144.5 (d, $^2J_{P,F}$ = 711 Hz). LRESI-MS (pos.): 1796.88, calc. for $[C_{116}H_{130}N_7O_{11}]^+$ = 1796.98.

Notes and references

^{a} Inorganic Chemistry Laboratory, Department of Chemistry, University of Oxford, South Parks Road, Oxford, United Kingdom, OX1 3QR.
^{b} Departamento de Química, CICECO and Secção Autónoma de Ciências da Saúde, Universidade de Aveiro, 3810-193 Aveiro (Portugal).
Electronic Supplementary Information (ESI) available: [General synthetic remarks, NMR and mass spectra of novel compounds, ROESY NMR spectrum of **7·PF$_6$**, titration protocols and binding data and further details of crystallography and modelling experiments. Full crystallographic data are provided in CIF format, and have been deposited with the Cambridge Structural Database, reference code: 997909]. See DOI: 10.1039/b000000x/

1 a) P. D. Beer and P. A. Gale, *Angew. Chem. Int. Ed.* 2001, **40**, 486; b) M. T. Albelda, J. C. Frías, E. García-España, H-J. Schneider, *Chem. Soc. Rev.* 2012, **41**, 3859.

2   P. A. Gale, *Chem. Commun.*, 2011, **47**, 82.

3   a) Y. Li and A. H. Flood, *Angew. Chem. Int. Ed.*, 2008, **47**, 2649; b) H. Juwarker, J. M. Lenhardt, D. M. Pham and S. L. Craig, *Angew. Chem. Int. Ed.*, 2008, **47**, 3740.

4   selected examples: a) H. Juwarker, J. M. Lenhardt, J. C. Castillo, E. Zhao, S. Krishnamurthy, S. Jamiolkowski, K-H. Kim andS. L. Craig, *J. Org. Chem.*, 2009, **74**, 8924; b) J. L. Sessler, J. J. Cai, H-Y. Gong, X. P. Yang, J. F. Arambula and B. P. Hay, *J. Am. Chem. Soc.*, 2010, **132**, 14058; c) K. P. McDonald, Y. Hua, S. Lee and A. H. Flood, *Chem. Commun.*, 2012, **48**, 5065; d) Y. Hua, Y. Liu, C-H. Chen and A. H. Flood, *J. Am. Chem. Soc.*, 2013, **135**, 14401; e) R. O. Ramabhadran, Y. Liu, Y. Hua, M. Ciardi, A. H. Flood and K. Raghavachari, *J. Am. Chem. Soc.*, 2014, **136**, 5078; f) B. Schulze and U. S. Schubert, *Chem. Soc. Rev.*, 2014, **43**, 2522.

5   a) A. Kumar and P. S. Pandey, *Org. Lett.*, 2008, **10**, 165; b) K. M. Mullen, J. Mercurio, C. J. Serpell and P. D. Beer, *Angew. Chem. Int. Ed.*, 2009, **48**, 4781; c) B. Schulze, C. Friebe, M. D. Hager, W. Gunther, W. Kohn, B. Jahn, H. Gorls and U. S. Schubert, *Org. Lett.*, 2010, **12**, 2710; d) A. Tripathi and P. S. Pandey, *Tetrahedron Lett.*, 2011, **52**, 3558; e) R. Chhatra, A. Kumar and P. S. Pandey, *J. Org. Chem.*, 2011, **76**, 9086; f) N. G. White, S. Carvalho, V. Félix and P. D. Beer, *Org. Biomol. Chem.*, 2012, **10**, 6951; g) L. C. Gilday, N. G. White and P. D. Beer, *Dalton Trans.*, 2012, **41**, 7092; h) G. T. Spence, M. B. Pitak and P. D. Beer, *Chem. Eur. J.*, 2012, **18**, 7100; i) J. J. Cai, B. P. Hay, N. J. Young, X. P. Yang and J. L. Sessler, *Chem. Sci.*, 2013, **4**, 1560; j) L. C. Gilday, N. G. White and P. D. Beer, *Dalton Trans.*, 2013, **42**, 15766; k) N. G. White, P. J. Costa, S. Carvalho, V. Félix and P. D. Beer, *Chem. Eur. J.*, 2013, **19**, 17751; l) N. G. White, H. G. Lovett and P. D. Beer, *RSC Adv.*, 2014, **4**, 12133.

6   Coutrot's group reported the first triazolium containing rotaxane, and have since reported several interlocked molecular shuttles and muscles containing triazolium groups: F. Coutrot and E. Busseron, *Chem. Eur. J.*, 2008, **14**, 4784.

7   Li, Li and co-workers have reported a series of acyclic anion receptors based on the amide-triazole motif: Y-J. Li, L. Xu, W-L. Yang, H-B. Liu, S-W. Lai, C-M. Che and Y-L. Li, *Chem. Eur. J.*, 2012, **18**, 4782.

8   N.G. White and P.D. Beer, *Org. Biomol. Chem.*, 2013, **11**, 1326.

9   H. W. Gibson, S-H. Lee, P. T. Engen, P. Lecavalier, J. Sze, Y. X. Shen and M. Bheda, *J. Org. Chem.*, 1993, **58**, 3748.

10 M. R. Sambrook, P. D. Beer, M. D. Lankshear, R. F. Ludlow and J. A. Wisner, *Org. Biomol. Chem.* 2006, **4**, 1529.

11 M. J. Hynes, *J. Chem. Soc., Dalton Trans.*, 1993, 311.

12 G. Trogdon, J. S. Murray, M. C. Concha and P. Politzer, *J. Mol. Model.*, 2007, **13**, 313.

13 Y. Ma, K. C. Gross, C. A. Hollingsworth, P. G. Seybold and J. S. Murray, *J. Mol. Model.*, 2004, **10**, 235.

14 a) N. Busschaert, S. J. Bradberry, M. Wenzel, C. J. E. Haynes, J. R. Hiscock, I. L. Kirby, L. E. Karagiannidis, S. J. Moore, N. J. Wells, J. Herniman, G. J. Langley, P. N. Horton, M. E. Light, I. Marques, P. J Costa, V. Félix, J. G. Frey and P. A. Gale, *Chem. Sci.*, 2013, **4**, 3036; b) C. J. Haynes, N. Busschaert, I. L. Kirby, J. Herniman, M. E. Light, N. J. Wells, I. Marques, V. Félix and P. A. Gale, *Org. Biomol. Chem.*, 2014, **12**, 62.

15 *Gaussian 09, Revision A.01*, M. J. Frisch, G. W. Trucks, H. B. Schlegel, G. E. Scuseria, M. A. Robb, J. R. Cheeseman, G. Scalmani, V. Barone, B. Mennucci, G. A. Petersson, H. Nakatsuji, M. Caricato, X. Li, H. P. Hratchian, A. F. Izmaylov, J. Bloino, G. Zheng, J. L. Sonnenberg, M. Hada, M. Ehara, K. Toyota, R. Fukuda, J. Hasegawa, M. Ishida, T. Nakajima, Y. Honda, O. Kitao, H. Nakai, T. Vreven, J. A. Montgomery, Jr., J. E. Peralta, F. Ogliaro, M. Bearpark, J. J. Heyd, E. Brothers, K. N. Kudin, V. N. Staroverov, R. Kobayashi, J. Normand, K. Raghavachari, A. Rendell, J. C. Burant, S. S. Iyengar, J. Tomasi, M. Cossi, N. Rega, J. M. Millam, M. Klene, J. E. Knox, J. B. Cross, V. Bakken, C. Adamo, J. Jaramillo, R. Gomperts, R. E. Stratmann, O. Yazyev, A. J. Austin, R. Cammi, C. Pomelli, J. W. Ochterski, R. L. Martin, K. Morokuma, V. G. Zakrzewski, G. A. Voth, P. Salvador, J. J. Dannenberg, S. Dapprich, A. D. Daniels, Ö. Farkas, J. B. Foresman, J. V. Ortiz, J. Cioslowski, and D. J. Fox, Gaussian, Inc., Wallingford CT, 2009.

16 It is important to note that inter-component preorganization will also play a significant role in determining binding strengths (see Ref. 5k), although in this case, given the similar size and shape of the axle components, differences in preorganization between the axle components should be small.

17 A. E. Reed, L. A. Curtiss and F. Weinhold, *Chem. Rev.*, 1988, **88**, 899.

18 J. A. Wisner, P. D. Beer, M. G. B. Drew and M. R. Sambrook, *J. Am. Chem. Soc.*, 2002, **124**, 12469.

19 H. Nowell, S. A. Barnett, K. E. Christensen, S. J. Teat and D. R. Allan, *J. Synchrotron Rad.*, 2012, **19**, 435.

20 K. Cosier and A. M. Glazer, *J. Appl. Crystallogr.*, 1986, **19**, 105.

21 *CrysAlis Pro*, Agilent Technologies, Yarnton, Oxfordshire, UK.

22 A. Altomare, G. Cascarano, C. Giacovazzo, M. C. Burla, G. Polidori and M. Camalli, *J. Appl. Crystallogr.*, 1994, **27**, 435.

23 P. W. Betteridge, J. R. Carruthers, R. I. Cooper, K. Prout and D. J. Watkin, *J. Appl. Crystallogr.*, 2003, **36**, 1487.

24 R. I. Cooper, A. L. Thompson and D. J. Watkin, *J. Appl. Crystallogr.*, 2010, **43**, 1017.

25 R. I. Cooper, R. O. Gould, S. Parsons and D. J. Watkin, *J. Appl. Crystallogr.*, 2002, **35**, 168.